Available online at www.sciencedirect.com
SCIENCE DIRECT®
ELSEVIER
International Journal of Solids and Structures 43 (2006) 3230–3253
INTERNATIONAL JOURNAL OF SOLIDS and STRUCTURES
www.elsevier.com/locate/ijsolstr

Static analysis of simply supported functionally graded and layered magneto-electro-elastic plates

Rajesh K. Bhangale [1], N. Ganesan *

Machine Design Section, Department of Mechanical Engineering, Indian Institute of Technology Madras, Chennai 600 036, India

Received 15 February 2005
Available online 18 July 2005

Abstract

In this article, static analysis of functionally graded, anisotropic and linear magneto-electro-elastic plates have been carried out by semi-analytical finite element method. A series solution is assumed in the plane of the plate and finite element procedure is adopted across the thickness of the plate such a way that the three-dimensional character of the solution is preserved. The finite element model is derived based on constitutive equation of piezomagnetic material accounting for coupling between elasticity, electric and magnetic effect. The present finite element is modeled with displacement components, electric potential and magnetic potential as nodal degree of freedom. The other fields are calculated by post-computation through constitutive equation. The functionally graded material is assumed to be exponential in the thickness direction. The numerical results obtained by the present model are in good agreement with available functionally graded three-dimensional exact benchmark solutions given by Pan and Han [Pan, E., Han, F., in press. Green's function for transversely isotropic piezoelectric functionally graded multilayered half spaces. Int. J. Solids Struct.]. Numerical study includes the influence of the different exponential factor, magneto-electro-elastic properties and effect of mechanical and electric type of loading on induced magneto-electro-elastic fields. In addition further study has been carried out on non-homogeneous transversely isotropic FGM magneto-electro-elastic plate available in the literature [Chen, W.Q., Lee, K.Y., Ding, H.J., 2005. On free vibration of non-homogeneous transversely isotropic magneto-electro-elastic plates].

Keywords: FGM; Magneto-electro-elastic; Static; Finite element

* Corresponding author. Tel.: +91 44 22578174/5171; fax: +91 44 22578502.
E-mail addresses: rajesh_phd@iitm.ac.in (R.K. Bhangale), nganesan@iitm.ac.in (N. Ganesan).
[1] Ph.D. Scholar, IIT Madras.

0020-7683/$ - see front matter © 2005 Published by Elsevier Ltd.
doi:10.1016/j.ijsolstr.2005.05.030

1. Introduction

Literature dealing with research on the behaviour of magneto-electro-elastic structures has gained more importance recently as these smart or intelligent materials have ability of converting energy from one form to the other (among magnetic, electric and mechanical energy) (Nan, 1994; Harshe et al., 1993). Such materials can exhibits field coupling that is not present in any of the monolithic constituent material. With application in ultrasonic imaging devices, sensors, actuators, transducers and many other emerging components, there is a strong need for theories or techniques that can predict the coupled response of theses so called smart materials, as well as structure composed of them. Studies on static and dynamic behaviour on plates as well as infinite cylinder has been dealt in the literature. Pan (2001) derived an exact closed-form solution for the simply supported and multilayered plate made of anisotropic piezoelectric and piezomagnetic materials under a static mechanical load. Pan and Heyliger (2002) solved the corresponding vibration problem. Piezoelectric and piezomagnetic composites exhibit coupling effect of electric and magnetic fields. In most of the studies these composite materials has been used as layers or as multiphase. The behaviour of finitely long cylindrical shells under uniform internal pressure has been studied by Wang and Zhong (2003) and they conclude that piezoelectric and Piezomagnetic composites in general have the coupling effect which is two orders higher than that of single-phase magnetoelectric constituent materials. Micro-mechanical analysis of fully coupled electro-magneto-thermo-elastic composites has been carried out by Aboudi (2001) for the prediction of the effective moduli of magneto-electro-elastic composites. Li (2000) studied the multi-inclusion and inhomogeneity problems in a magneto-electro-elastic solid. From the literature survey, it is found that only few studies have been reported on magneto-electro-elastic structures by finite element analysis. Free vibration behaviour of infinitely long magneto-electro-elastic cylindrical shell has been studied by Buchanan (2003) by using semi-analytical finite element method. Buchanan (2004) has studied the behaviour of layered versus multiphase magneto-electro-elastic infinite long plate composites by finite element method. Wang et al. (2003) derived the state vector approach to analysis of multilayered magneto-electro-elastic plates for mechanical and electrical loading. Lage et al. (2004) developed a layerwise partial mixed finite element model for magneto-electro-elastic plate. The studies on non-homogeneous magneto-electro-elastic structure are less in the literature. Chen and Lee (2003) adopted state space formulation to derive equations for non-homogeneous transversely isotropic magneto-electro-elastic plates. According to Chen et al. (2005), like other advanced material the functionally graded magneto-electro-elastic structures will be appear soon and they carried out free vibration analysis of non-homogeneous transversely isotropic magneto-electro-elastic plates.

The special feature of graded spatial compositions (non-homogeneous) associated with FGM provides freedom in the design and manufacturing of novel structures. Still it is great challenges in the numerical modeling and simulation of the FGM structure (Liew et al., 2003; Pan and Han, in press).

Recently Pan and Han (2005) presented an exact solution for functionally graded and layered magneto-electro-elastic plates by Pseudo-Stroh formalism and they mentioned that their results can serve as a benchmarks for finite element and boundary element solutions of the problem. Hence in the present study, static analysis of functionally graded and layered magneto-electro-elastic plates has been carried out by using series solution in conjunction with finite element approach. In addition the main aim of the study is to evaluate the influence of functionally grading on the mechanical, electrical and magnetic behaviour.

2. Constitutive equations

The coupled constitutive equations for anisotropic and linearly magneto-electro-elastic solids can be written as

$$\sigma_k = C_{jk}S_k - e_{kj}E_k - q_{kj}H_k \tag{1}$$

$$D_k = e_{jk}S_k + \varepsilon_{jk}E_k + m_{jk}H_k \tag{2}$$

$$B_j = q_{jk}S_k + m_{jk}E_k + \mu_{jk}H_k \tag{3}$$

where σ_k denotes stress, D_j is the electric displacement and B_j is the magnetic induction. C_{jk}, ε_{jk} and μ_{jk} are the elastic, dielectric and magnetic permeability coefficients. e_{kj}, q_{kj} and m_{jk} are piezoelectric, piezomagnetic and magnetoelectric material coefficients. Apparently, various uncoupled cases can be reduced from Eqs. (1)–(3). A completely coupled magneto-electro-elastic material matrix, assuming a hexagonal crystal class, for above constitutive equations given below by Buchanan (2003):

$$\begin{Bmatrix} \sigma_1 \\ \sigma_2 \\ \sigma_3 \\ \sigma_4 \\ \sigma_5 \\ \sigma_6 \\ D_1 \\ D_2 \\ D_3 \\ B_1 \\ B_2 \\ B_3 \end{Bmatrix} = \begin{bmatrix} C_{11} & C_{12} & C_{13} & 0 & 0 & 0 & 0 & 0 & e_{31} & 0 & 0 & q_{31} \\ C_{12} & C_{11} & C_{13} & 0 & 0 & 0 & 0 & 0 & e_{31} & 0 & 0 & q_{31} \\ C_{13} & C_{13} & C_{33} & 0 & 0 & 0 & 0 & 0 & e_{33} & 0 & 0 & q_{33} \\ 0 & 0 & 0 & C_{44} & 0 & 0 & 0 & e_{15} & 0 & 0 & q_{15} & 0 \\ 0 & 0 & 0 & 0 & C_{44} & 0 & e_{15} & 0 & 0 & q_{15} & 0 & 0 \\ 0 & 0 & 0 & 0 & 0 & C_{66} & 0 & 0 & 0 & 0 & 0 & 0 \\ 0 & 0 & 0 & 0 & e_{15} & 0 & \varepsilon_{11} & 0 & 0 & m_{11} & 0 & 0 \\ 0 & 0 & 0 & e_{15} & 0 & 0 & 0 & \varepsilon_{11} & 0 & 0 & m_{11} & 0 \\ e_{31} & e_{31} & e_{33} & 0 & 0 & 0 & 0 & 0 & \varepsilon_{33} & 0 & 0 & m_{33} \\ 0 & 0 & 0 & 0 & q_{15} & 0 & m_{11} & 0 & 0 & \mu_{11} & 0 & 0 \\ 0 & 0 & 0 & q_{15} & 0 & 0 & 0 & m_{11} & 0 & 0 & \mu_{11} & 0 \\ q_{31} & q_{31} & q_{33} & 0 & 0 & 0 & 0 & 0 & m_{33} & 0 & 0 & \mu_{33} \end{bmatrix} \begin{Bmatrix} S_1 \\ S_2 \\ S_3 \\ S_4 \\ S_5 \\ S_6 \\ E_1 \\ E_2 \\ E_3 \\ H_1 \\ H_2 \\ H_3 \end{Bmatrix} \tag{4}$$

The strain–displacement relations are

$$\begin{aligned} &\sigma_{xx} = \sigma_1 = \frac{\partial u}{\partial x}; \quad \sigma_{yy} = \sigma_2 = \frac{\partial v}{\partial y}; \quad \sigma_{zz} = \sigma_3 = \frac{\partial w}{\partial z} \\ &\sigma_{yz} = \sigma_4 = \frac{\partial v}{\partial z} + \frac{\partial w}{\partial y}; \quad \sigma_{xz} = \sigma_5 = \frac{\partial u}{\partial z} + \frac{\partial w}{\partial x}; \quad \sigma_{xy} = \sigma_6 = \frac{\partial u}{\partial y} + \frac{\partial v}{\partial x} \end{aligned} \tag{5}$$

where u, v and w are mechanical displacements in coordinate directions x, y and z.

The electric field vector E_i is related to the electric potential Φ as shown below:

$$E_x = E_1 = -\frac{\partial \phi}{\partial x}; \quad E_\theta = E_2 = -\frac{\partial \phi}{\partial y}; \quad E_z = E_3 = -\frac{\partial \phi}{\partial z} \tag{6}$$

The magnetic field H_i is related to magnetic potential ψ as shown below:

$$H_x = H_1 = -\frac{\partial \psi}{\partial x}; \quad H_\theta = H_2 = -\frac{\partial \psi}{\partial y}; \quad H_z = H_3 = -\frac{\partial \psi}{\partial z} \tag{7}$$

3. Finite element formulation

Recently Buchanan (2004) has analyzed free vibration behaviour for infinitely long plate. In the present work finite series solution has been assumed satisfying boundary conditions for simply supported plates has been adopted. The finite element model has been used in the thickness direction. For a general loading the shape functions are as follows:

$$
\begin{aligned}
u(x,y,z) &= \sum_{n=1}^{N}\sum_{m=1}^{M} U_{nm}(z)\cos\left(\frac{n\pi}{L_x}\right)x\sin\left(\frac{m\pi}{L_y}\right)y \\
v(x,y,z) &= \sum_{n=1}^{N}\sum_{m=1}^{M} V_{nm}(z)\sin\left(\frac{n\pi}{L_x}\right)x\cos\left(\frac{m\pi}{L_y}\right)y \\
w(x,y,z) &= \sum_{n=1}^{N}\sum_{m=1}^{M} W_{nm}(z)\sin\left(\frac{n\pi}{L_x}\right)x\sin\left(\frac{m\pi}{L_y}\right)y \\
\varphi(x,y,z) &= \sum_{n=1}^{N}\sum_{m=1}^{M} \Phi_{nm}(z)\sin\left(\frac{n\pi}{L_x}\right)x\sin\left(\frac{m\pi}{L_y}\right)y \\
\psi(x,y,z) &= \sum_{n=1}^{N}\sum_{m=1}^{M} \Psi_{nm}(r)\sin\left(\frac{n\pi}{L_x}\right)x\sin\left(\frac{m\pi}{L_y}\right)y
\end{aligned}
\tag{8}
$$

where n and m being two positive integers and N and M are the number of terms in the series to be accounted for the general loading. In the present study analysis has been carried out similar to the reported by Pan and Han (2005) for $m = n = 1$. In the end the analysis has been reduced for finite element in thickness direction still retaining the three-dimensional dependence the solution based on the choice of n and m. The analysis is carried out by two noded finite element and the assumed shape functions are

$$U_i = [N_u]\{U\}; \quad \Phi = [N_\varphi]\{\Phi\}; \quad \Psi = [N_\varphi]\{\Psi\} \tag{9}$$

where

$$N_1 = \left(1 - \frac{z_i}{z_{i+1} - z_i}\right); \quad N_2 = \left(\frac{z_i}{z_{i+1} - z_i}\right)$$

For a coupled filed problem finite element equations are as follows:

$$
\begin{aligned}
&[K_{uu}]\{U\} + [K_{u\phi}]\{\phi\} + [K_{u\psi}]\{\psi\} = 0 \\
&[K_{u\phi}]^{\mathrm{T}}\{U\} - [K_{\phi\phi}]\{\phi\} - [K_{\phi\psi}]\{\psi\} = 0 \\
&[K_{u\psi}]^{\mathrm{T}}\{U\} - [K_{\phi\psi}]^{\mathrm{T}}\{\phi\} - [K_{\psi\psi}]\{\psi\} = 0
\end{aligned}
\tag{10}
$$

Various stiffness matrices are defined as shown below:

$$
\begin{aligned}
[K_{uu}] &= c\int [B_u]^{\mathrm{T}}[C][B_u]\,\mathrm{d}z \\
[K_{u\phi}] &= c\int [B_u]^{\mathrm{T}}[e][B_\phi]\,\mathrm{d}z \\
[K_{u\psi}] &= c\int [B_u]^{\mathrm{T}}[q][B_\psi]\,\mathrm{d}z \\
[K_{\phi\phi}] &= c\int [B_\phi]^{\mathrm{T}}[\varepsilon][B_\phi]\,\mathrm{d}z \\
[K_{\psi\psi}] &= c\int [B_\psi]^{\mathrm{T}}[\mu][B_\psi]\,\mathrm{d}z \\
[K_{\phi\psi}] &= c\int [B_\phi]^{\mathrm{T}}[m][B_\psi]\,\mathrm{d}z
\end{aligned}
\tag{11}
$$

where $C = 0.25L_xL_y$.

$[B_u]$, $[B_\phi]$, $[B_\psi]$ represents the strain–displacement, electric field–electric potential and magnetic field–magnetic potential relations respectively. The component matrices for Eq. (11) are

$$[B_u] = [L_u][N_u] = \begin{bmatrix} \frac{\partial}{\partial x} & 0 & 0 \\ 0 & \frac{\partial}{\partial y} & 0 \\ 0 & 0 & \frac{\partial}{\partial z} \\ 0 & \frac{\partial}{\partial z} & \frac{\partial}{\partial y} \\ \frac{\partial}{\partial z} & 0 & \frac{\partial}{\partial x} \\ \frac{\partial}{\partial y} & \frac{\partial}{\partial x} & 0 \end{bmatrix} \times \begin{bmatrix} N_1 & 0 & 0 & N_2 & 0 & 0 \\ 0 & N_1 & 0 & 0 & N_2 & 0 \\ 0 & 0 & N_1 & 0 & 0 & N_2 \end{bmatrix} \tag{12}$$

$$[B_u] = \begin{bmatrix} -\left(\frac{n\pi}{L_x}\right)N_1 & 0 & 0 & \cdots \\ 0 & -\left(\frac{m\pi}{L_x}\right)N_1 & 0 & \cdots \\ 0 & 0 & \frac{\partial N_1}{\partial z} & \cdots \\ 0 & \frac{\partial N_1}{\partial z} & \left(\frac{m\pi}{L_x}\right)N_1 & \cdots \\ \frac{\partial N_1}{\partial z} & 0 & \left(\frac{n\pi}{L_x}\right)N_1 & \cdots \\ \left(\frac{m\pi}{L_x}\right)N_1 & \left(\frac{n\pi}{L_x}\right)N_1 & 0 & \cdots \end{bmatrix} \tag{13}$$

where there are three additional columns for N_2. The matrix $[B_\phi]$ is developed using Eq. (6) and is as follows:

$$[B_\phi] = [L_\phi][N_\phi] = \begin{bmatrix} \frac{\partial}{\partial x} \\ \frac{\partial}{\partial y} \\ \frac{\partial}{\partial z} \end{bmatrix} [N_1 \quad N_2] = \begin{bmatrix} -\left(\frac{n\pi}{L_x}\right)N_1 & -\left(\frac{n\pi}{L_x}\right)N_2 \\ -\left(\frac{m\pi}{L_y}\right)N_1 & -\left(\frac{m\pi}{L_y}\right)N_2 \\ \frac{\partial N_1}{\partial z} & \frac{\partial N_2}{\partial z} \end{bmatrix} \tag{14}$$

Similarly for Eq. (7) gives

$$[B_\psi] = [L_\psi][N_\psi] = \begin{bmatrix} \frac{\partial}{\partial x} \\ \frac{\partial}{\partial y} \\ \frac{\partial}{\partial z} \end{bmatrix} [N_1 \quad N_2] = \begin{bmatrix} -\left(\frac{n\pi}{L_x}\right)N_1 & -\left(\frac{n\pi}{L_x}\right)N_2 \\ -\left(\frac{m\pi}{L_y}\right)N_1 & -\left(\frac{m\pi}{L_y}\right)N_2 \\ \frac{\partial N_1}{\partial z} & \frac{\partial N_2}{\partial z} \end{bmatrix} \tag{15}$$

In the present study the Gaussian integration scheme has been implemented to evaluate integrals involved in different matrices. The functionally graded material properties based on the assumptions made as described in the next section are accounted by evaluating the material properties at Gaussian points.

Problem has been solved by decoupled way. In the case of mechanical load the conventional elastic stiffness matrix of the system has been inverted to obtain the mechanical displacements. Neglecting the coupling between magnetic and piezoelectric the system of equation pertaining to be solved to obtain the potential in the plate, based on the mechanical displacements. Similarly magnetic potential has been evaluated by considering the coupling between displacements and magnetic.

4. Analytical model of FGM materials properties

4.1. Functionally and layered magneto-electro-elastic plate

First to start with validation of the present formulation the layered FGM plate (Model-I) made up of three layers is considered reported by Pan and Han (2005). The three layers have equal thickness of 0.1 m and the horizontal dimensions of the plate are $L_x \times L_y = 1\text{ m} \times 1\text{ m}$. Two functionally graded and layered sandwich plates with stacking sequence $BaTiO_3/COFe_2O_4/BaTiO_3$ (B/F/B) and $CoFe_2O_4/BaTiO_3/COFe_2O_4$ (F/B/F) are shown in Fig. 1(a). Both top and bottom layers are functionally graded with the symmetric exponential variation as shown in Fig. 1(b). Five different exponential factors, i.e., $\eta = -10, -5, 0, 5, 10$ (1/m), were studied.

The functionally graded material with exponential variation in the thickness direction (z-direction), the material coefficients are given by

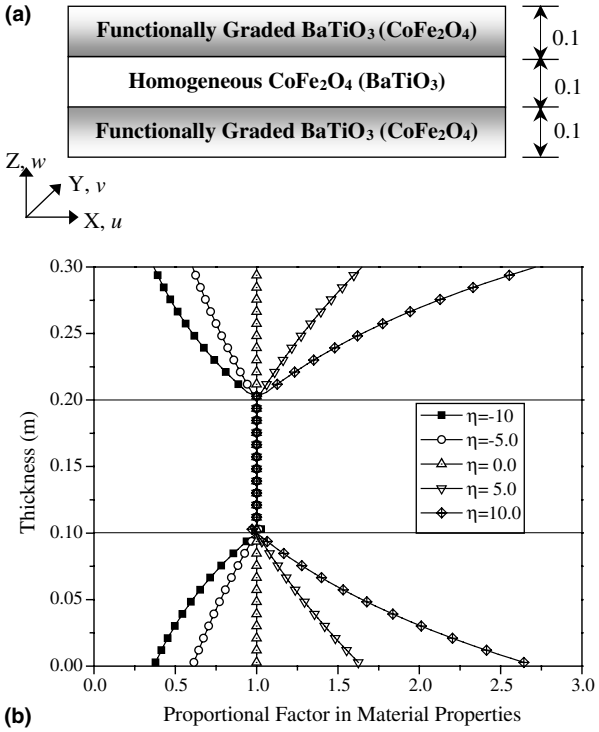

Fig. 1. (a) Coordinate and configuration of functionally graded and layered magneto-electro-elastic plate under study (Model-I). (b) Variation of FGM proportional coefficient ($e^{\eta z}$) across the thickness of the FGM and layered plate.

$$C_{ik}(z) = C^0_{ik}e^{\eta z}; \quad e_{ik}(z) = e^0_{ik}e^{\eta z}; \quad q_{ik}(z) = q^0_{ik}e^{\eta z}$$
$$\varepsilon_{ik}(z) = \varepsilon^0_{ik}e^{\eta z}; \quad \mu_{ik}(z) = \mu^0_{ik}e^{\eta z}; \quad d_{ik}(z) = d^0_{ik}e^{\eta z} \tag{16}$$

where η is the exponential factor governing the degree of the material gradient in the z-direction, and the superscript 0 is attached to indicate the z-independent factors in the material coefficients. For $\eta = 0$ corresponds to the homogeneous material case.

4.2. Functionally graded (non-homogeneous) magneto-electro-elastic plate

Further study has been carried out for non-homogeneous transversely isotropic FGM magneto-electro-elastic plate reported in the literature (Chen et al., 2005). The present study considers functionally graded material composed of piezoelectric and magnetostrictive material. The grading is accounted across the thickness of the FGM magneto-electro-elastic plate as shown in Fig. 2(a). An advantage of a plate made of a FGM over a laminated plate is that material properties vary continuously in a FGM but are discontinuous across the adjoining layers in a laminated plate. This has been achieved by grading the volume fraction of particular material governed by power law index. Fig. 2(b) depicts the through-the-thickness distribution of the volume fraction for different power law indexes n. Consider an FGM magneto-

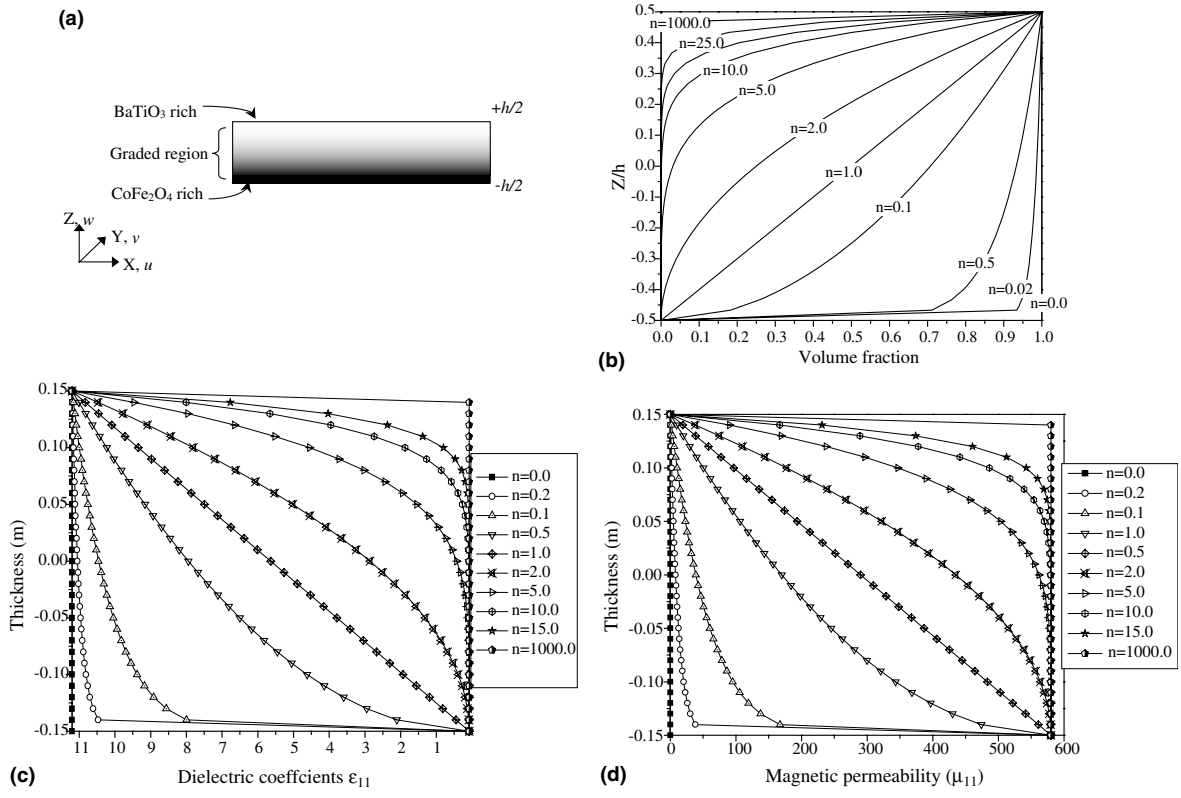

Fig. 2. (a) Coordinate and configuration of functionally graded magneto-electro-elastic plate (Model-II). (b) Through-the-thickness distribution of the volume fraction for different values of the power law index n. (c) Variations of effective dielectric constants of magnetostrictive material along the thickness direction of functionally graded plate (Model-II). (d) Variations of effective magnetic permeability constants of magnetostrictive material along the thickness direction of Functionally graded plate (Model-II).

electro-elastic plate having horizontal dimensions L_x and $L_y = 1\text{ m} \times 1\text{ m}$ and thickness $h = 0.3$. In the present analysis it is assumed that the composition is varied from the bottom surfaces to top surface, i.e., the top surface of the plate is piezoelectric-rich, whereas the bottom surface is magnetostrictive-rich. In addition material properties are graded throughout the thickness direction according to volume fraction power law distribution. Present study considers smooth and continuous variation of the volume fraction of either piezoelectric or magnetostrictive material governed by the power law index.

A simple power law type definition for the volume fraction of the metal across the thickness direction of the FGM plate is assumed as given in Eq. (17):

$$V_B = \left(\frac{2z+h}{2h}\right)^n \tag{17}$$

where h is the thickness of the plate, z is the thickness coordinates ($0 \leqslant z \leqslant h$), and n is the power law index. The bottom surface of the plate ($z = -h/2$) is $CoFe_2O_4$-rich whereas the top surface ($z = h/2$) of the plate is $BaTiO_3$-rich. The sum total volume of the constituent materials, $BaTiO_3(B)$ and $CoFe_2O_4(F)$ should be

$$V_B + V_C = 1 \tag{18}$$

Based on the volume fraction definition and law of mixtures, the effective material property definition follows:

$$(\text{MP})_{\text{eff}} = (\text{MP})_{\text{top}} V_B + (\text{MP})_{\text{bottom}} V_C \tag{19}$$

'MP' is general notation for material property. Making use of Eqs. (17)–(19) the following effective elastic, piezoelectric, piezomagnetic, dielectric and magnetic permeability, and thermal properties definitions can be written as

$$C_{\text{eff}} = (C_B - C_F)\left(\frac{2z+h}{2h}\right)^n + C_F \tag{20a}$$

$$e_{\text{eff}} = (e_B - e_F)\left(\frac{2z+h}{2h}\right)^n + e_F \tag{20b}$$

$$q_{\text{eff}} = (q_B - q_F)\left(\frac{2z+h}{2h}\right)^n + q_F \tag{20c}$$

$$\varepsilon_{\text{eff}} = (\varepsilon_B - \varepsilon_F)\left(\frac{2z+h}{2h}\right)^n + \varepsilon_F \tag{20d}$$

$$\mu_{\text{eff}} = (\mu_B - \mu_F)\left(\frac{2z+h}{2h}\right)^n + \mu_F \tag{20e}$$

In Eqs. (20a)–(20e), 'eff' stands for effective material properties obtained by above equations for particular power law index n. Material coefficients of the piezoelectric $BaTiO_3$ and magnetostrictive $CoFe_2O_4$ is given in Appendix. In addition variation of effective dielectric coefficients and effective magnetic permeability with respect to power law index n across the thickness direction is shown in Fig. 2(c) and (d). It is seen that for power law index $n = 1.0$ the variation of effective material property is linear.

5. Result and discussion

In this section, we present some numerical results by using the present finite element formulation used in this paper. First a benchmark problem (Pan and Han, 2005) is considered for validating the present finite

element method. Second another functionally graded model available in the literature (Chen et al., 2005) is considered subjected to both mechanical and electric loading.

5.1. Mechanical load on the top surface of the functionally graded and layered plate

A simply supported FGM and layered square plate of thickness 0.3 m is subjected to a distributed load on a top surface with the sinusoidal distribution $\sin(\pi/L_x)\sin(\pi/L_y)$. Consistent load vector approach is used in finite element sense to evaluate the response of the system. Responses are calculated for fixed horizontal coordinates $(x, y) = (0.75L_x, 0.25L_y)$.

Fig. 3(a) and (b) shows the variation of the in plane elastic displacement u_x $(=-u_y)$ in the FGM B/F/B and F/B/F respectively. It is seen that as exponential factor 'η' is decreases magnitude of horizontal displacement u_x increases. This behaviour is similar on the top and bottom surfaces. In addition it is noticed that variation of elastic displacements is similar for both stacking sequence with slight difference in magnitude. Magnitude of the elastic displacements in B/F/B is larger than that of F/B/F. Fig. 3(c) and (d) shows the elastic displacement u_z for B/F/B and F/B/F respectively. Vertical displacement u_z increases with decreasing of exponential factor in a plate. Here $\eta = 0$ pertains to homogeneous B/F/B and F/B/F plates reported by Pan (2001), Wang et al. (2003) and Lage et al. (2004) and it is found that present results are in good correlations observed between them. Fig. 4(a) and (b) shows the variation of the ϕ electric potential

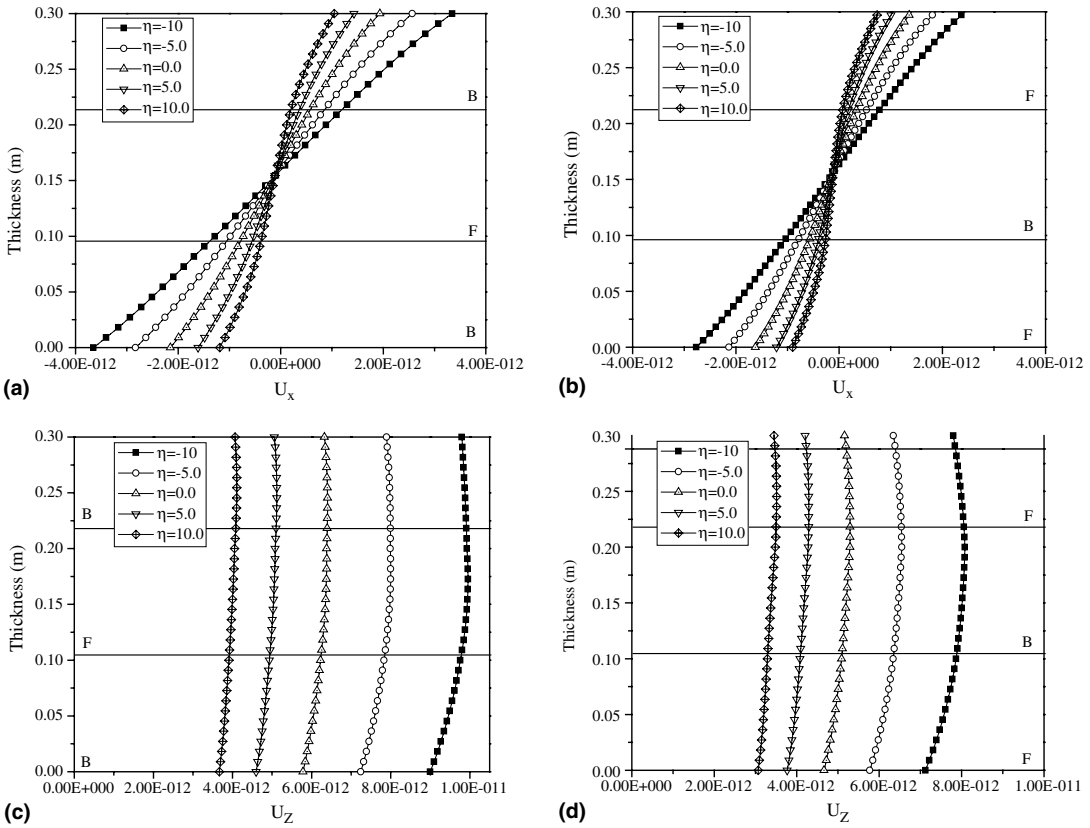

Fig. 3. Elastic displacement components $u_x$and u_z (m) variation across the thickness direction in FGM magneto-electro-elastic plate.

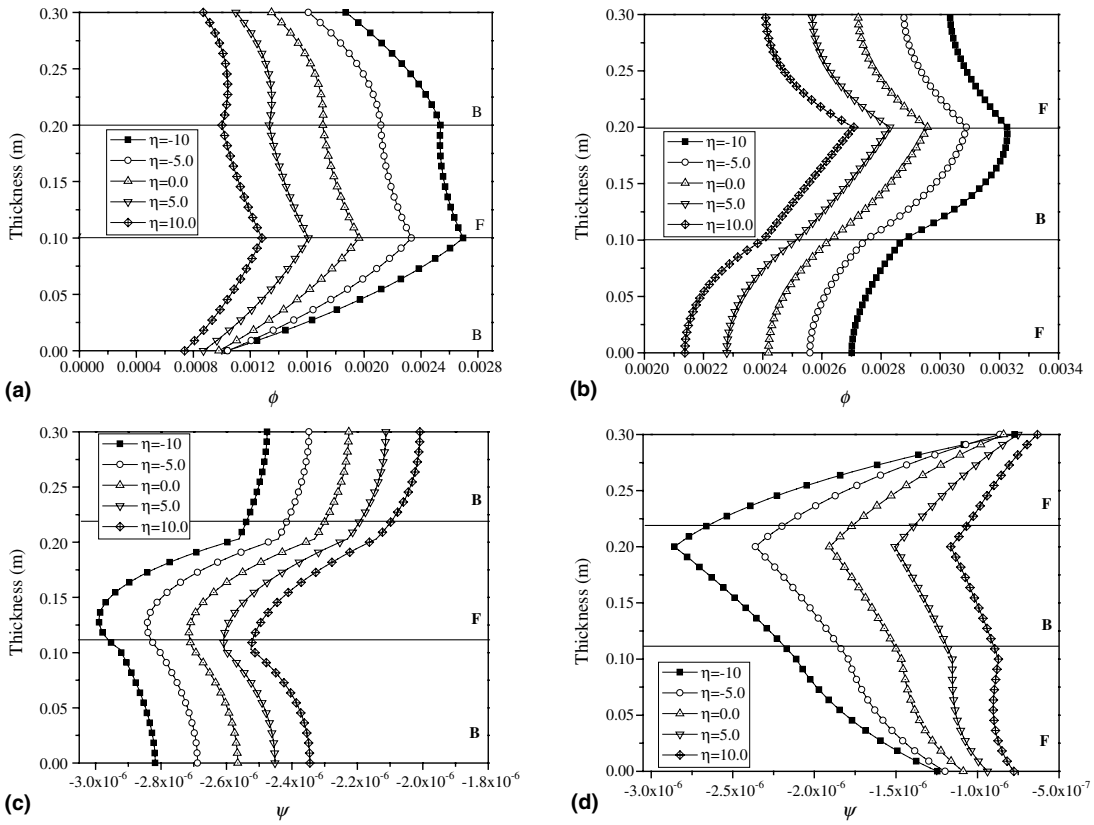

Fig. 4. Electric potential ϕ (V) and magnetic potential ψ (C/s) distribution across the thickness in FGM magneto-electro-elastic plate for different exponential factor caused by a mechanical load acts on the top surface: ϕ in (a) and ψ in (c) for B/F/B, and ϕ in (b) and ψ in (d) for F/B/F.

for B/F/B and F/B/F cases across the thickness direction. While Fig. 4(c) and (d) shows the variation of magnetic potential ψ across the thickness for the B/F/B and F/B/F cases. As exponential factor 'η' increases the magnitude of the electric and magnetic potential decreases. In addition it is noticed that slope of the potentials are discontinuous across the thickness even though potentials are continuous.

Fig. 5(a) and (b) shows the distribution of stress component σ_{xx} ($=\sigma_{yy}$) across the thickness direction for B/F/B and F/B/F stacking sequence respectively. It is observed that the horizontal stress is discontinuous across the interfaces and it is very sensitive to the exponential factor 'η'.

Fig. 5(c) and (d) shows the variation of σ_{zz} for the B/F/B and F/B/F. It is apparent that both stacking sequences produce nearly the same stress distribution pattern, even though elastic constants for the two materials are considerably different. Please see Appendix. Fig. 6(a) and (b) shows the shear stress variation across the thickness. It is seen that both stacking sequence produce nearly the similar pattern and magnitude of B/F/B is slightly larger.

Fig. 7(a–b) and (c–d) show the electric displacements D_x ($=-D_y$) and D_z, and the magnetic induction B_x ($=-B_y$) and B_z are shown in Fig. 8(a–b) and (c–d) for B/F/B and F/B/F cases. It is observed that electric displacement and magnetic inductions are very much sensitive for different exponential factor 'η'. Further it is noticed that because of material property discontinues in different layer the horizontal electric displacement and magnetic induction are discontinuous across the interface.

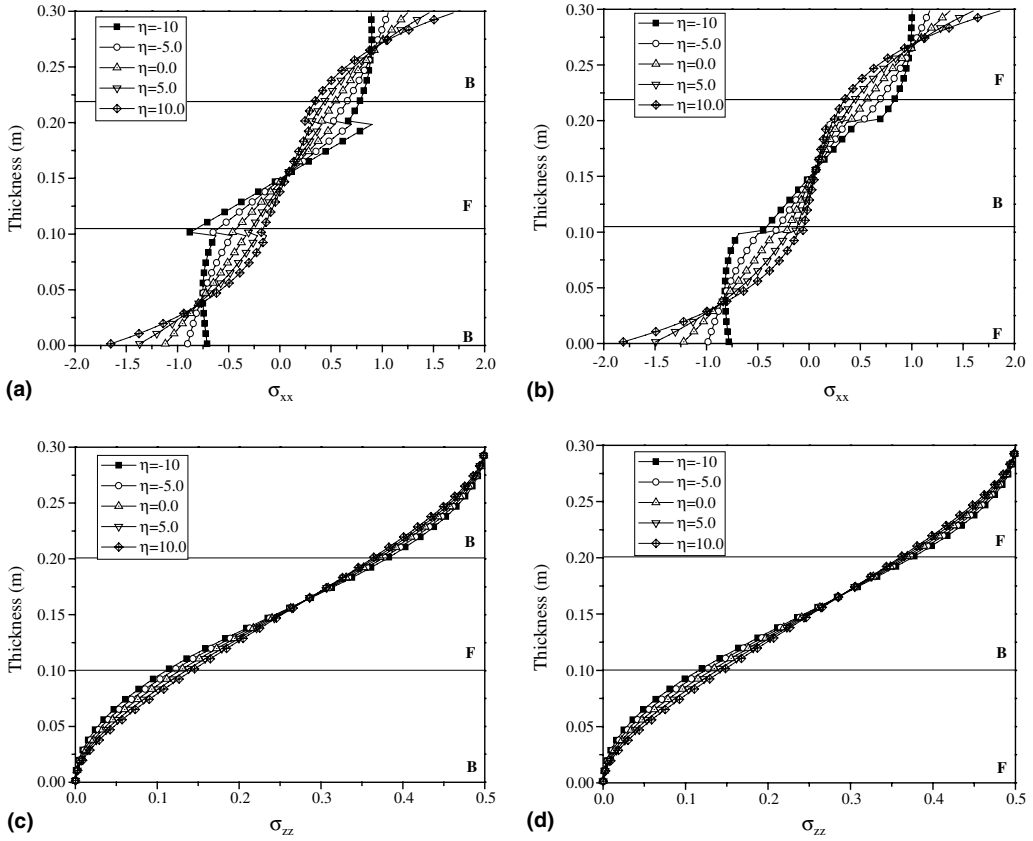

Fig. 5. Stress component distribution σ_{xx} and σ_{zz} (N/m^2) across the thickness direction: σ_{xx} in (a) and σ_{zz} in (c) for the B/F/B, and σ_{xx} in (b) and σ_{zz} in (d) for F/B/F case.

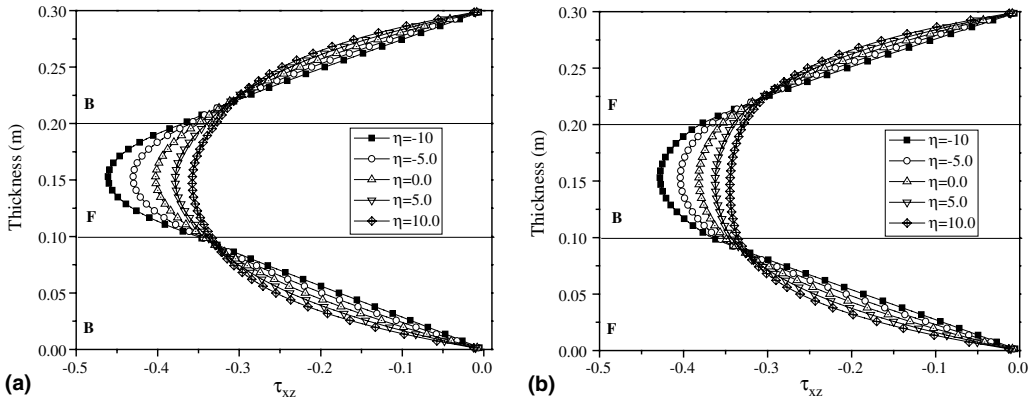

Fig. 6. Variation of the shear stress across the thickness direction: τ_{xz} in (a) for B/F/B and τ_{xz} in (b) for F/B/F.

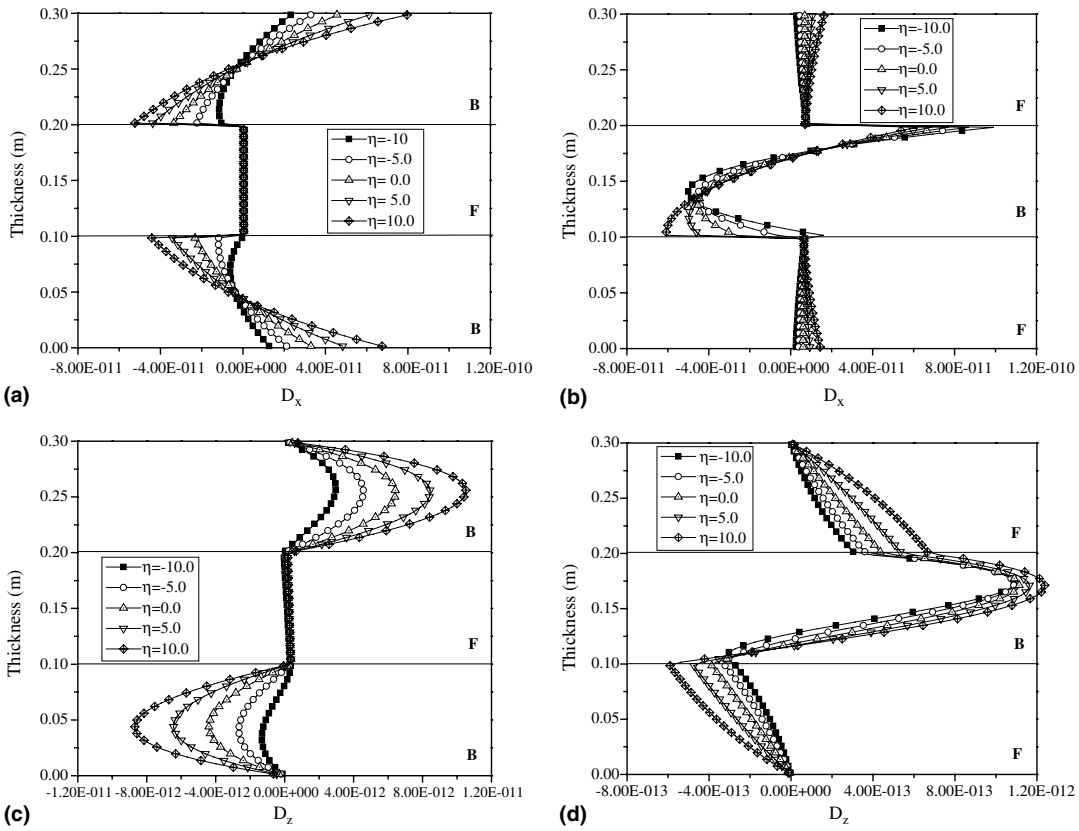

Fig. 7. Electric displacements components D_x and D_z (C/m^2) along the thickness direction in FGM magneto-electro-elastic plate for different exponential factor caused by a mechanical load acts on the top surface: D_x in (a) and D_z in (c) for the B/F/B case, and D_x in (b) and D_z in (d) for the F/B/F case.

5.2. Electrical potential (load) on the top surface of the functionally graded and layered plate

The FGM magneto-electro-elastic plate is loaded electrically on the top surface of sinusoidal distribution $\phi = \phi_0 \sin(\pi/L_x)\sin(\pi/L_y)$ by an amount of $\phi_0 = 1$ V. The response has been calculated at same location i.e. horizontal coordinate fixed at $(x, y) = (0.75L_x, 0.25L_y)$.

Fig. 9(a) and (b) shows the distribution of the elastic displacement u_x $(=-u_y)$ in the FGM B/F/B and F/B/F cases in plate. Fig. 9(c) and (d) shows the elastic displacement u_z for B/F/B and F/B/F respectively. It is noticed that elastic displacements in the plate are completely dissimilar as compared to caused by mechanical load. In addition influence of stacking sequence has been felt.

The variation of the magnetic potential ψ across the thickness of the FGM B/F/B and F/B/F plate has been shown in Fig. 10(a) and (b). It is noticed that magnitude of the magnetic potential in B/F/B is higher than that of F/B/F. In addition it is felt that for actuation purpose the large magnitude potential can be induced in bottom layer under the influence of electric potential on top surface.

Fig. 11(a) and (b) shows the distribution of the stress components σ_{xx} $(=-\sigma_{yy})$ across the thickness of the plate for B/F/B and F/B/F cases respectively. The effect of stacking sequence has been felt on the stress components both in terms of curved shape and magnitude as compared to mechanical load reported in Fig. 5. Effect of exponential factor has been felt in graded layers (top and bottom) for both stacking

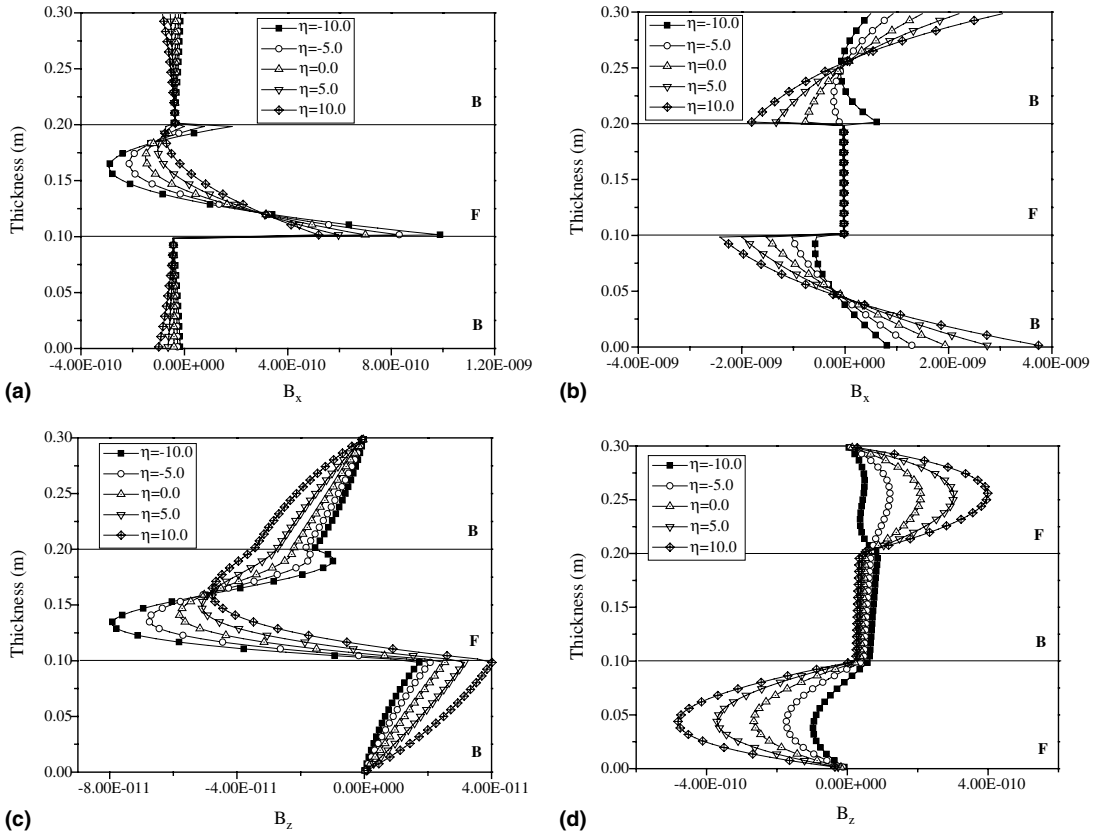

Fig. 8. Magnetic induction components B_x and B_z (Wb/m^2) along the thickness direction in FGM magneto-electro-elastic plate for different exponential factor caused by a mechanical load acts on the top surface: B_x in (a) and B_z in (c) for the B/F/B case, and B_x in (b) and B_z in (d) for F/B/F case.

sequence. Fig. 11(c) and (d) shows the variation of shear stress across the thickness. It is seen that both stacking sequence produce different pattern and magnitude of F/B/F is larger than B/F/B.

Fig. 12(a–b) and (c–d) show the electric displacements D_x ($=-D_y$) and D_z, and the magnetic induction B_x ($=-B_y$) and B_z are shown in Fig. 13(a–b) and (c–d) for B/F/B and F/B/F cases. Here also stacking sequence plays an important role in terms of shape and magnitude of the electric displacement and magnetic induction. In addition it is seen that electric displacement effect is felt more in top layers as compared to other under the application of electric potential. This is hold good for both stacking sequences. In addition it is observed the discontinuity at the interfaces of the layers. Regarding the magnetic induction in F/B/F case a relatively large magnetic field can be still induced in the magnetostrictive layer even if an electric load is applied in the case of F/B/F case. Similar observations have been reported by Pan and Han (2005).

5.3. Mechanical loading on the top surface of the FGM plate (Model-II)

The FGM plate is subjected to mechanical load on the top surface with the following sinusoidal distribution. $\sin(\pi/L_x)\sin(\pi/L_y)$; $\sigma_0 = 1$ N/m^2 at fixed horizontal coordinates $(x, y) = (0.75L_x, 0.25L_y)$. Consistent load vector approach has been used. Fig. 14(a) and (b) shows the variation of the inplane elastic displacement u_x ($=-u_y$) and u_z in the FGM magneto-electro-elastic plate for different power law index 'n'.

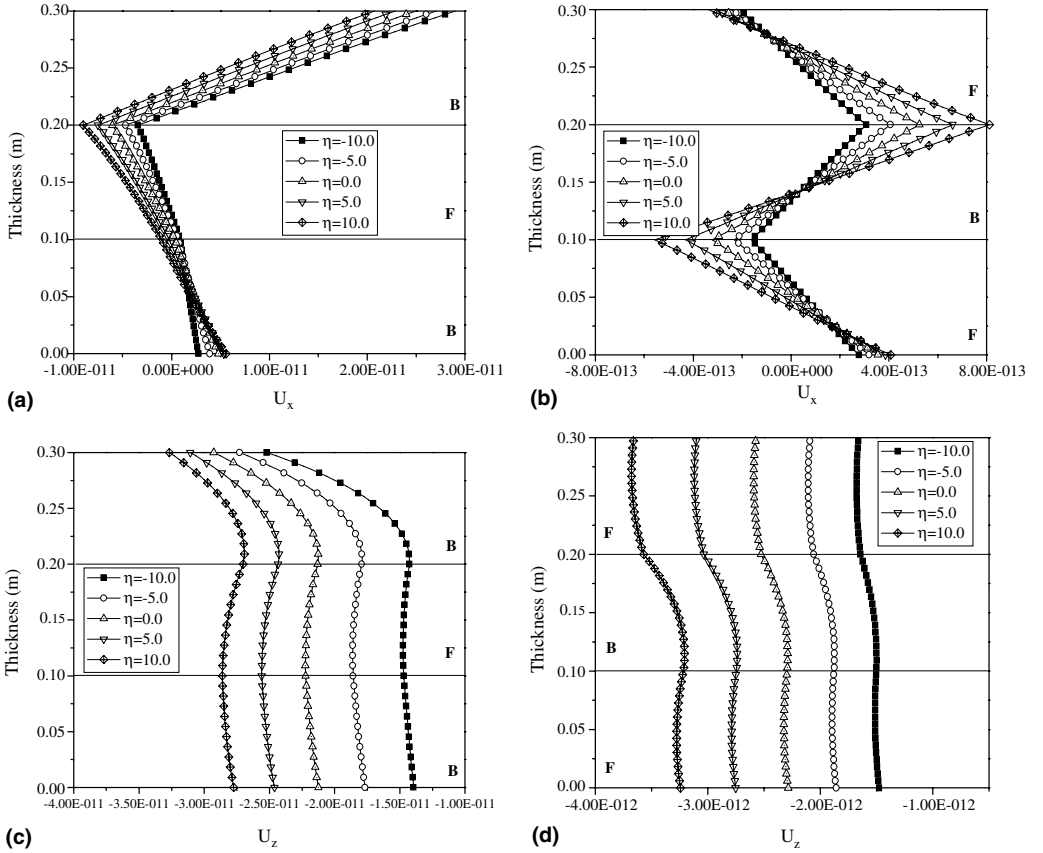

Fig. 9. Elastic displacement components u_x and u_z (m) distribution across the thickness direction in FGM magneto-electro-elastic plate for different exponential factor caused by an electric potential on the top surface: u_x in (a) and u_z in (b) for B/F/B, and u_x in (c) and u_z in (d) for F/B/F.

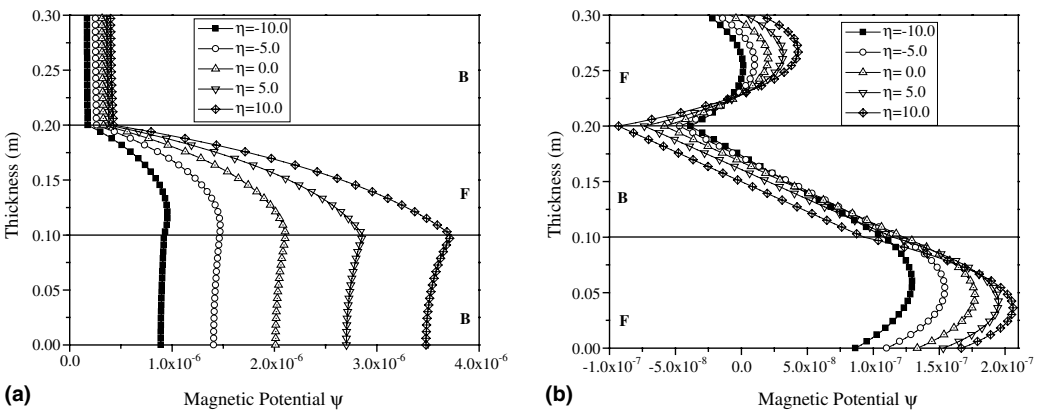

Fig. 10. Magnetic potential ψ (C/s) distribution across the thickness in FGM magneto-electro-elastic plate: ψ in (a) for B/F/B and ψ in (b) for F/B/F.

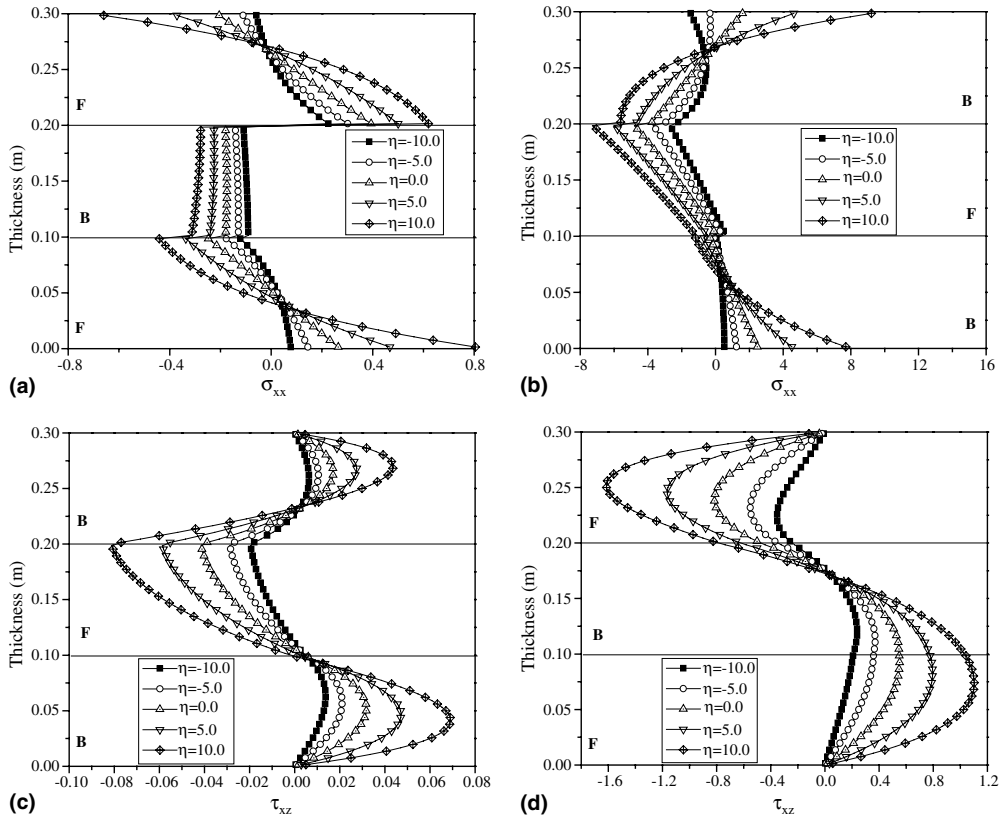

Fig. 11. Stress component distribution σ_{xx} and τ_{xz} across the thickness direction of FGM plate: σ_{xx} in (a) for the B/F/B, and σ_{xx} in (b) for F/B/F case; τ_{xz} in (c) for the B/F/B and (d) for F/B/F case.

Here $n = 0.0$ corresponds to homogeneous piezoelectric material ($BaTiO_3$) while $n = 1000.0$ corresponds to magnetostrictive materials ($CoFe_2O_4$). The power law index value n other than two extreme values governs the distribution of properties of $BaTiO_3$ and $CoFe_2O_4$ mixture in FGM magneto-electro-elastic plate. Variation of the composition of piezoelectric and magnetostrictive is linear for power law index $n = 1.0$. It is seen that as power law index n decreases the magnitude of horizontal displacement u_x and u_z increases, as it is approaching towards the homogeneous $BaTiO_3$. This phenomenon can be explained by looking at elastic properties of both structures, as elastic modulus of the $BaTiO_3$ is smaller than the $CoFe_2O_4$. This behaviour is similar on the top and bottom surfaces. The other power law index behaviour is lies between the two extreme homogeneous materials.

Fig. 15(a) and (b) shows the variation of the ϕ electric potential and magnetic potential ψ across the thickness direction for FGM plate. It is seen that as electric potential ϕ increases as decrease in power law index. It is interesting to note that the magnitude of electric potential is very small for power law index $n = 1000.0$. This is due to the fact that for pure magnetostrictive materials, piezoelectric (e_{ij}) coefficients are zero. In case of magnetic potential distribution as power law index increases the magnitude of ψ increases from $n = 0.0$ and attains maximum at $n = 1000.0$. In case of magnetostrictive material the piezoelectric coefficients (q_{ij}) are zero. Fig. 16(a) and (b) shows the distribution of stress component σ_{xx} ($=\sigma_{yy}$) and σ_z across the thickness direction in Fig. 17 for FGM plate. It is seen that magnitude of σ_z is around 2.5 times of the inplane stresses. Inplane stresses are predominant as compared to normal stress. Further it is seen that all power law index will produce nearly the same magnitude for σ_z. Fig. 18(a) and (b) shows

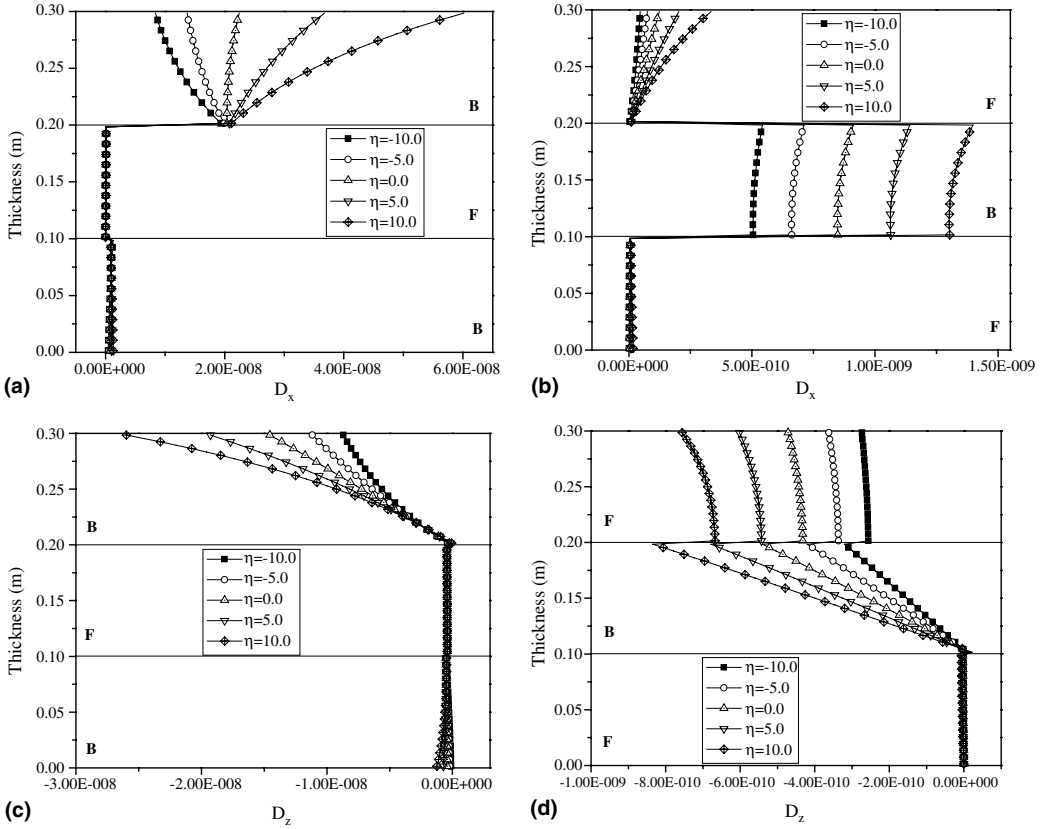

Fig. 12. Electric displacements components D_x and D_z (C/m^2) along the thickness direction in FGM magneto-electro-elastic plate for different exponential factor caused by a mechanical load acts on the top surface: D_x in (a) and D_z in (b) for the B/F/B case, and D_x in (c) and D_z in (d) for the F/B/F case.

the electric displacements D_x ($=-D_y$) and D_z, and the magnetic induction B_x ($=-B_y$) and B_z are shown in Fig. 19(a) and (b) for FGM magneto-electro-elastic plate. It is observed that electric displacement and magnetic inductions are very much sensitive for different power law index. For $n = 0.0$ the magnitude of electric displacement is higher and then it reduces slowly as increase in n and finally reduces to zero for $n = 1000.0$. The magnitude is higher at top surface. While magnetic induction is higher for $n = 1000.0$ and then reduces slowly as decrease in power law index and finally becomes zero for $n = 0.0$ (piezoelectric material). In addition it is observed that there is a dramatic variation of the electric displacement and magnetic induction across the thickness of the FGM plate.

In the literature mainly the study deals with the influence of mechanical load on the displacement, stresses, electric potential, magnetic potential, electric displacement and magnetic induction. The maximum absolute values of different quantities for different power law index n are listed in Table 1 caused by mechanical load. Generally use of these materials as sensing devices is to be attempted. It is felt that for a sensor it is preferable to have maximum electric potentials if electric quantities is used to be a sensor. As expected for $n = 0.0$ electric potential is maximum. In contrast it is preferable to use $n = 1000.0$ if magnetic field is used as a sensor. Intermediate value of n will better if both the magnetic and electric potential used for the sensing. From this study it may possible to choose appropriate for grading governed by power law index depending on applications.

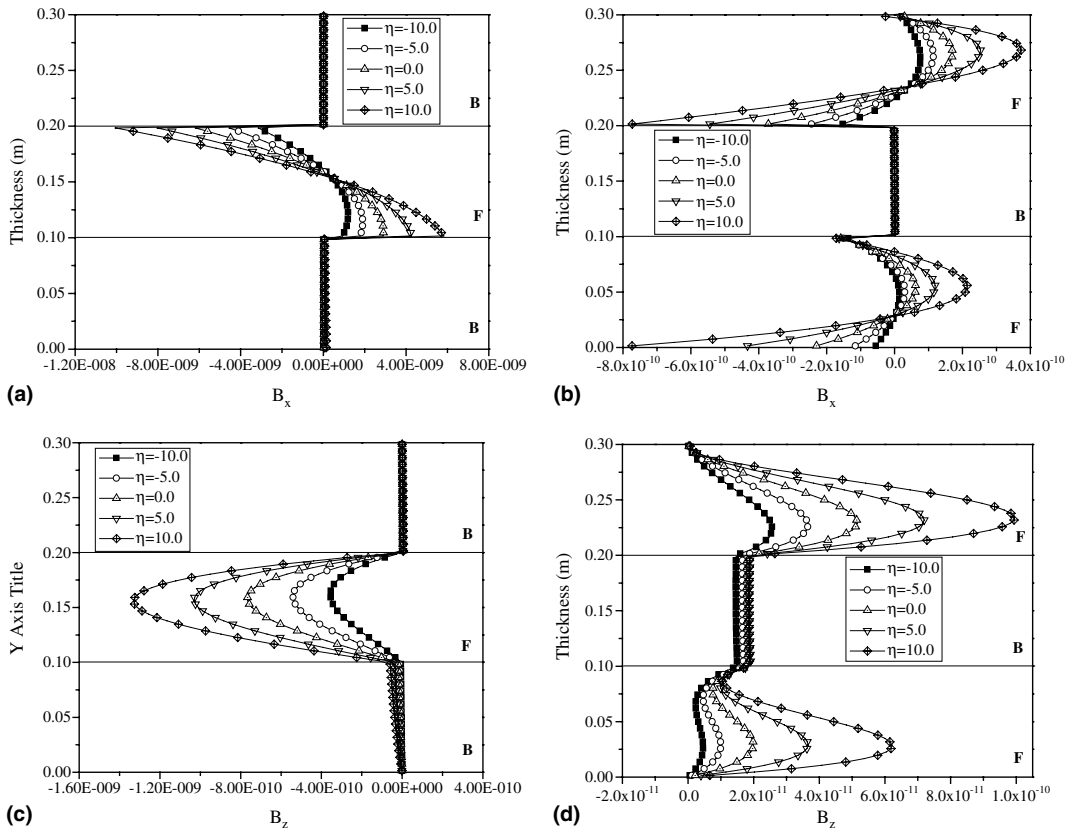

Fig. 13. Magnetic induction components B_x and B_z (Wb/m^2) along the thickness direction in FGM magneto-electro-elastic plate for different exponential factor caused by a mechanical load acts on the top surface: B_x in (a) and B_z in (b) for the B/F/B case, and B_x in (c) and B_z in (d) for F/B/F case.

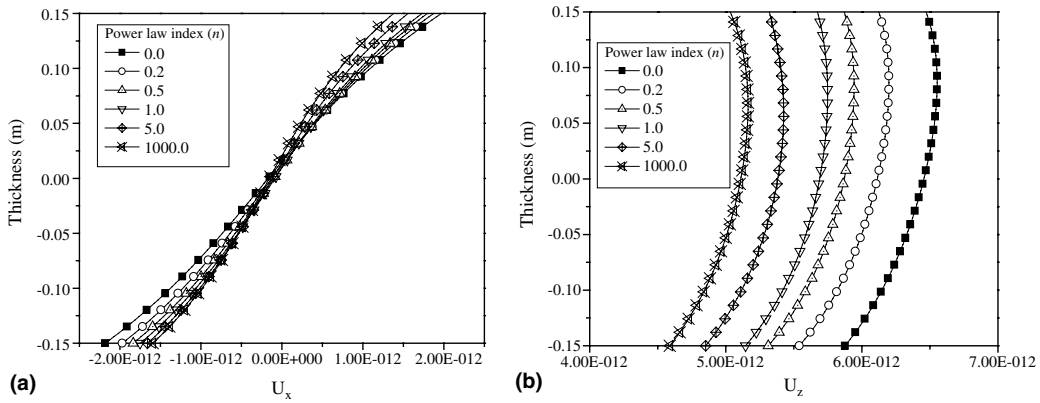

Fig. 14. Elastic displacement variation across the thickness: (a) U_x and (b) U_z.

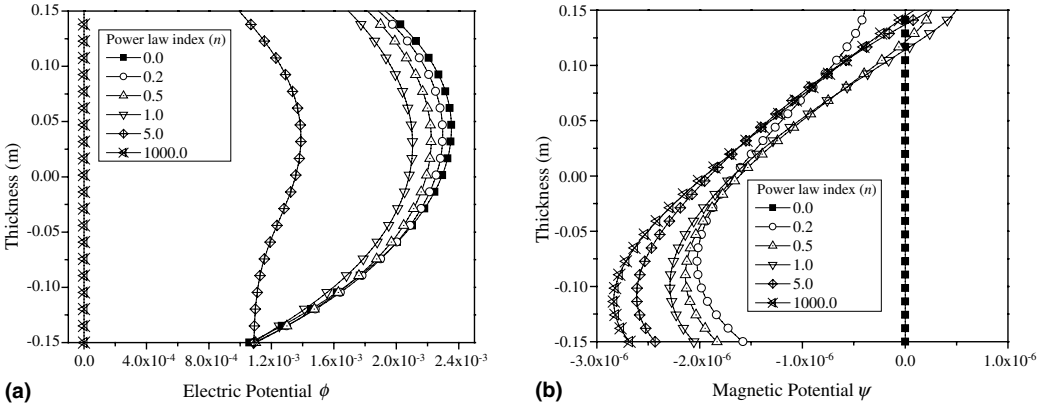

Fig. 15. Potential distribution across the thickness: (a) electric and (b) magnetic.

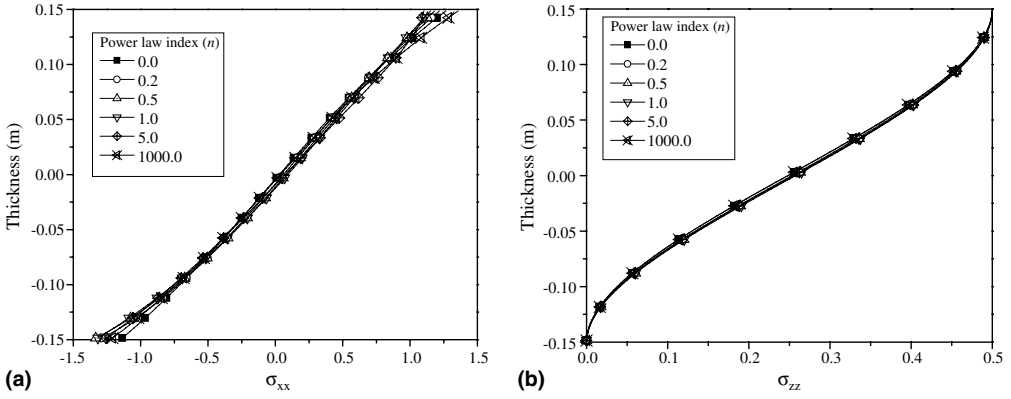

Fig. 16. Stress variation across the FGM plate thickness: (a) σ_{xx} and (b) σ_{zz}.

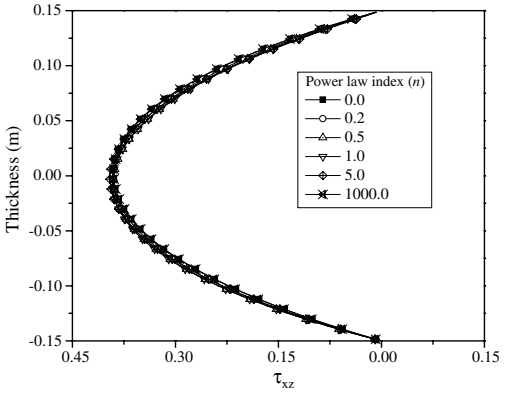

Fig. 17. Variation of shear stress across the thickness of FGM plate.

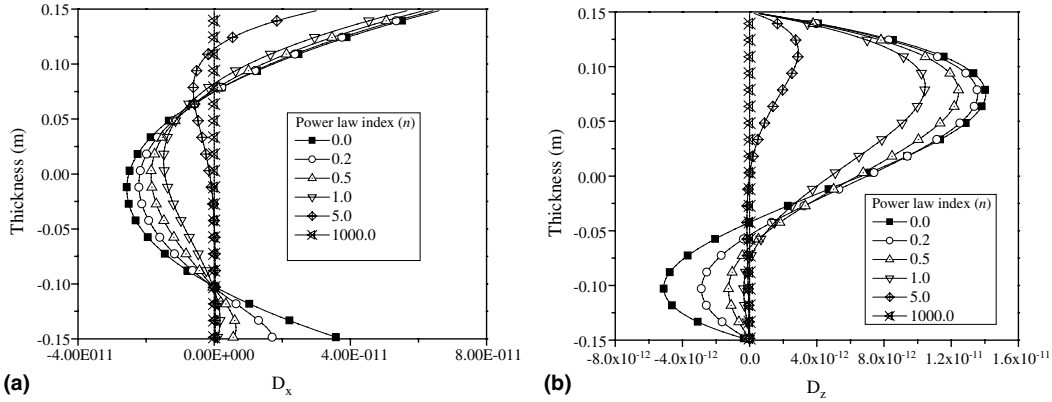

Fig. 18. Variation of electric displacement across the thickness of plate: (a) D_x and (b) D_z.

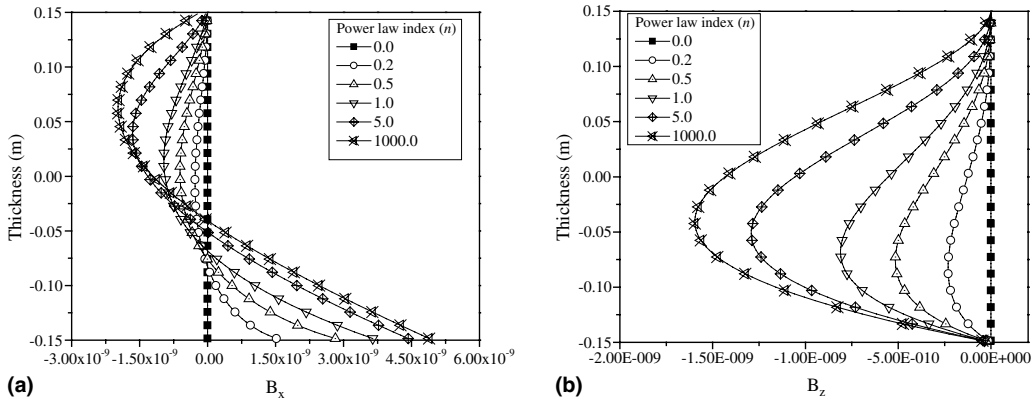

Fig. 19. Variation of magnetic induction across the thickness of plate: (a) B_x and (b) B_z.

5.4. Electrical potential (load) on the top surface of the FGM plate (Model-II)

The FGM magneto-electro-elastic plate is loaded electrically on the top surface of sinusoidal distribution $\phi = \phi_0 \sin(\pi/L_x)\sin(\pi/L_y)$ by an amount of $\phi_0 = 1$V. The response has been calculated at same location i.e. horizontal coordinate fixed at $(x, y) = (0.75L_x, 0.25L_y)$. Consistent load vector approach is used in finite element sense to evaluate the response of the system.

Fig. 20(a) and (b) shows the distribution of the elastic displacement u_x $(=-u_y)$ in the FGM plate. It is noticed that elastic displacements pattern in the plate are completely dissimilar as compared to caused by mechanical load. For power law index $n = 0.0$ the maximum inplane displacements has been noticed and subsequently there is decrease in displacements as increase in the power law index, $n = 1000.0$ there is minimum elastic displacement. This fact can be explained by looking at the properties of magnetostrictive material where piezoelectric coefficients are zero and the present study magneto electric coupling has been neglected.

Fig. 21(a) shows the variation of the ϕ electric potential for FGM plate across the thickness direction. As n increases the magnitude of electric potential is increases and attains maximum for $n = 5.0$. Further it is note that magnitude of all power law indexes is 0.5 at the top surface of the plate. Fig. 21(b) shows the

Table 1
Results for simply supported FGM plate (Model-II) with applied mechanical sinusoidal traction

$x = 0.75$, $y = 0.25$	$n = 0.0$ ($BaTiO_3$)	$n = 0.2$	$n = 1.0$	$n = 5.0$	$n = 1000.0$ ($CoFe_2O_4$)
u_x [m]	-2.18×10^{-12}	-1.97×10^{-12}	-1.75×10^{-12}	-1.66×10^{-12}	-1.37×10^{-12}
u_y [m]	2.18×10^{-12}	1.97×10^{-12}	1.75×10^{-12}	1.66×10^{-12}	1.37×10^{-12}
w [m]	6.55×10^{-12}	6.19×10^{-12}	5.74×10^{-12}	5.42×10^{-12}	5.16×10^{-12}
ϕ [V]	0.00235	0.0023	0.0021	0.00139	1.27×10^{-12}
ψ [C/s]	0.0	-3.93×10^{-7}	-2.30×10^{-6}	-2.61×10^{-6}	-2.84×10^{-6}
σ_{xx} [Pa]	1.26	1.21	1.15	1.10	1.35
σ_{yy} [Pa]	−1.26	−1.21	−1.15	−1.10	−1.35
σ_{zz} [Pa]	0.49	0.49	0.49	0.49	0.49
σ_{zx} [Pa]	−0.396	−0.389	−0.391	−0.395	−0.389
D_x [C/m^2]	-2.56×10^{-11}	-2.21×10^{-11}	-1.48×10^{-11}	-6.14×10^{-12}	0.0
D_x [C/m^2]	2.56×10^{-11}	2.21×10^{-11}	1.48×10^{-11}	6.14×10^{-12}	0.0
D_z [C/m^2]	1.40×10^{-11}	1.35×10^{-11}	1.04×10^{-11}	2.89×10^{-12}	0.0
B_x [Wb/m^2]	0.0	1.51×10^{-9}	3.64×10^{-9}	4.42×10^{-9}	4.88×10^{-9}
B_x [Wb/m^2]	0.0	-1.51×10^{-9}	-3.64×10^{-9}	-4.42×10^{-9}	-4.88×10^{-9}
B_z [Wb/m^2]	0.0	-2.31×10^{-9}	-8.10×10^{-9}	-1.29×10^{-9}	-1.59×10^{-9}

Maximum (in absolute value) across the thickness computed at $x = 0.75$, $y = 0.25$.

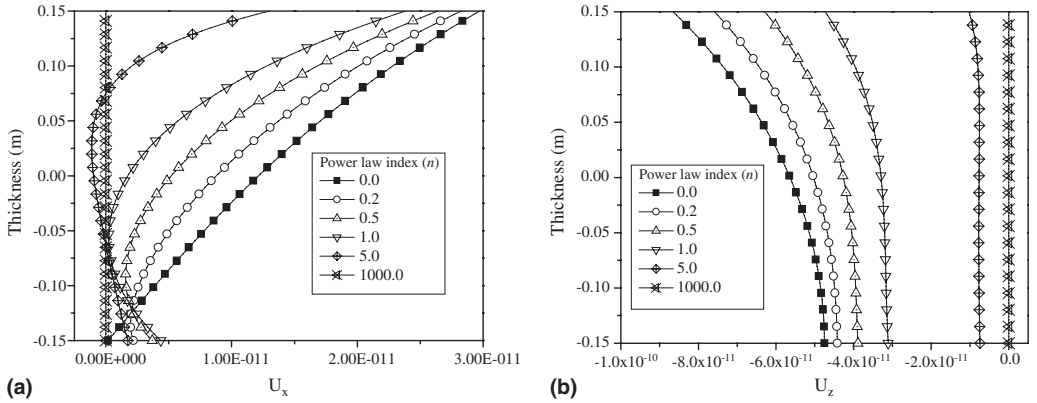

Fig. 20. Elastic displacement variation across the thickness: (a) U_x and (b) U_z.

variation of the magnetic potential across the thickness direction. It is seen that ψ vary dramatically across the thickness of the FGM plate.

Fig. 22(a) and (b) shows the distribution of the stress components σ_{xx} ($=-\sigma_{yy}$) and σ_{zz} across the thickness of the FGM plate respectively. It is observed that for $n = 0.0$ the magnitude of σ_{xx} is higher. This phenomenon has been expected as the elastic displacements are higher for $n = 0.0$. In case of σ_{zz} distribution it is seen that magnitude of stress distribution is higher for power law index $n = 1.0$ where the composition variation is linear for functionally graded magneto-electro-elastic material. In contrast to mechanical load here completely different magnitude and pattern of stresses has been observed.

Fig. 23(a) and (b) shows the electric displacements D_x ($=-D_y$) and D_z, and the magnetic induction B_x ($=-B_y$) and B_z are shown in Fig. 24(a) and (b) for FGM magneto-electro-elastic plate. It is observed that electric displacement and magnetic inductions are very much sensitive for different power law index. For $n = 0.0$ the magnitude of electric displacement is higher and then it reduces slowly as increase in n and

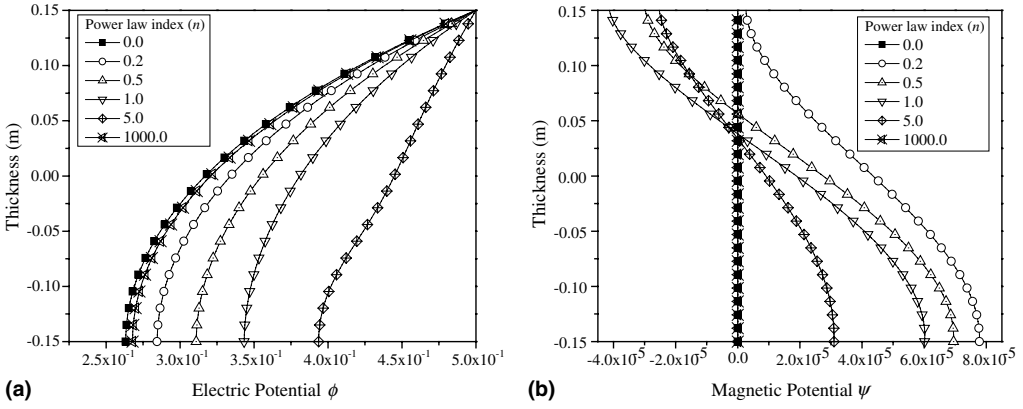

Fig. 21. Potential distribution across the thickness: (a) electric and (b) magnetic.

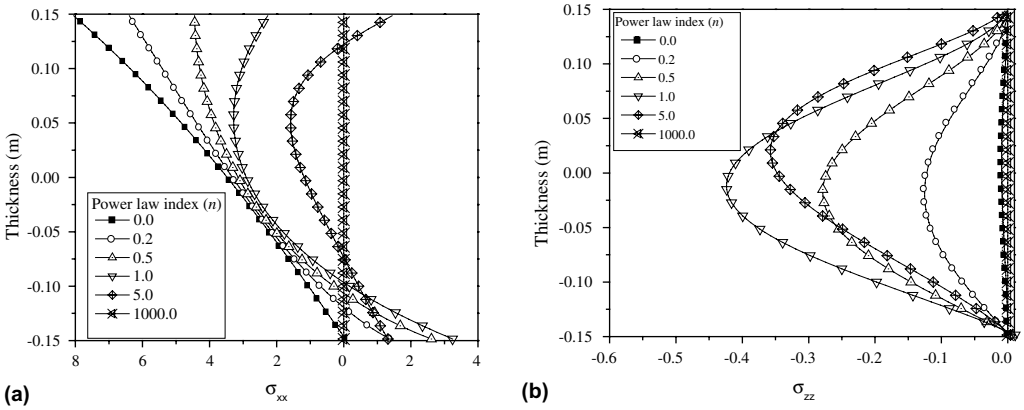

Fig. 22. Stress variation across the thickness of FGM plate: (a) σ_{xx} and (b) σ_{zz}.

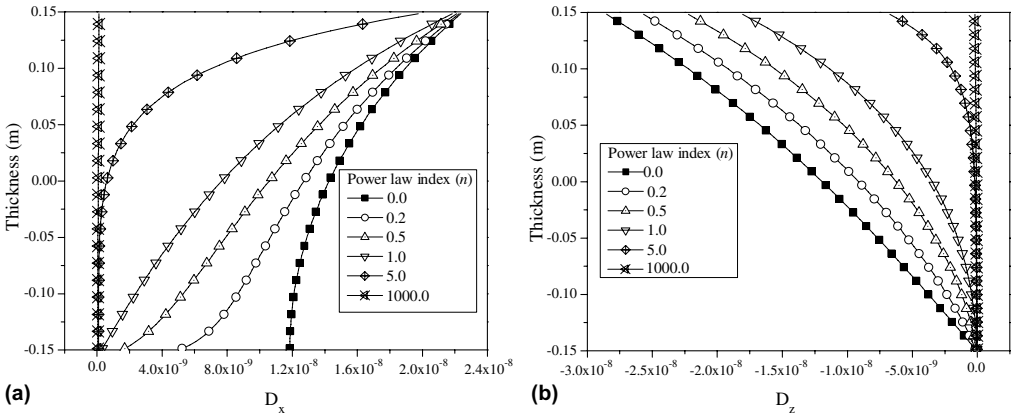

Fig. 23. Variation of electric displacement across the thickness of plate: (a) D_x and (b) D_z.

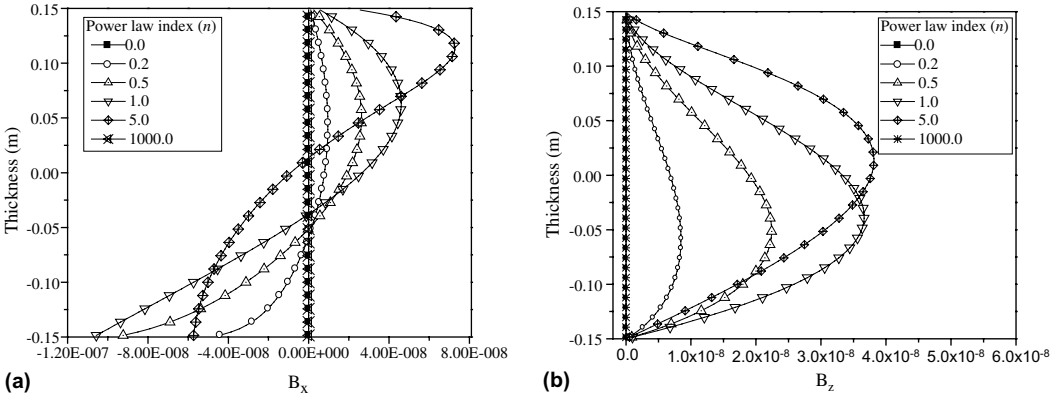

Fig. 24. Variation of magnetic induction across the thickness of plate: (a) B_x and (b) B_z.

Table 2
Material coefficients of the magneto-electro-elastic plate

	$CoFe_2O_4$	$BaTiO_3$
C_{11}	286	166
C_{12}	173	77
C_{13}	170	78
C_{33}	269.5	162
C_{44}	45.3	43
e_{15}	0	11.6
e_{31}	0	−4.4
e_{33}	0	18.6
ε_{31}	0.08	11.2
ε_{33}	0.093	12.6
μ_{11}	−5.9	0.05
μ_{33}	1.57	0.1
q_{15}	560	0
q_{31}	580	0
q_{33}	700	0
m_{11}	0	0
m_{33}	0	0

C_{ij} in 10^9 N/m^2, e_{ij} in C/m^2, ε_{ij} in 10^{-9} C/V m, q_{ij} in N/(A m), μ_{ij} in 10^{-4} N s^2/C^2, m_{ij} in 10^{-9} N s/V C.

finally reduces to zero for $n = 1000.0$. Magnetic induction is zero for the $n = 0.0$ and then magnitude increases and attains maximum at $n = 5.0$ and finally reduces to zero for $n = 1000.0$. This is due to the coupling between piezoelectric and magnetostrictive material has been neglected in the present study. Magnetic induction changes dramatically across the thickness of the FGM plate.

6. Conclusion

A series solution is assumed in the plane of the plate and finite element procedure is adopted across the thickness of the plate to solve the magneto-electro-elastic plate under mechanical and electrical loading.

The model is derived based on constitutive equation of piezomagnetic material. Coupling between elasticity, electric and magnetic effects are included in the analysis. The magneto electric coupling is neglected. The results of the present model are in good agreement with the exact benchmark solution for functionally graded and layered magneto-electro-elastic plate given by Pan and Han (2005). The FGM plate is graded in the thickness direction and a simple power law index will govern the magneto-electric constituents profile across the thickness. It is found that different exponential factors in Functionally graded and layered plate (Model-I) and different power law index in functionally graded plate (Model-II) produce different magnitudes of the response curve. As compare to mechanical loading, the electric potential produce completely different normal stress components distribution for different exponential factor and different power law index. In addition stacking sequences have substantial effect on the induced magnetic, electric, and elastic fields. The advantage of functionally graded material model over the layered model is that there is no discontinuity between the electric, magnetic, electric displacement and magnetic induction between the layers. It is felt that the present numerical study is highly useful for characterising FGM magneto-electro-elastic system for use as a sensors or actuators.

Acknowledgement

Authors would like to thank Professor E. Pan and F. Han, Department of Civil Engineering, University of Akron, OH, USA for giving valuable suggestion and providing literature.

Appendix

See Table 2.

References

Buchanan, G.R., 2003. Free vibration of an infinite magneto-electro-elastic cylinder. J. Sound Vib. 268, 413–426.

Buchanan, G.R., 2004. Layered verses multiphase magneto-electro-elastic composites. Composites B (Engg) 35, 413–420.

Chen, W.Q., Lee, K.Y., 2003. Alternative state space formulations for magneto electric thermo elasticity with transverse isotropy and the application to bending analysis of nonhomogeneous plate. Int. J. Solids Struct. 33 (7), 977–990.

Chen, W.Q., Lee, K.Y., Ding, H.J., 2005. On free vibration of non-homogeneous transversely isotropic magneto-electro-elastic plates. J. Sound Vib. 279, 237–251.

Harshe, G., Dougherty, J.P., Newnham, R.E., 1993. Theoretical modeling of multilayered magnetoelectric composites. Int. J. Appl. Electromag. Mater. 4, 145–159.

Lage, G.R., Soares, C.M., Soares, C.A., Reddy, J.N., 2004. Layer wise partial mixed finite element analysis of magneto-electro-elastic plates. Comput. Struct. 76, 299–317.

Li, J.Y., 2000. Magnetoelectroelastic multi-inclusion and inhomogeneity problems and their applications in composite materials. Int. J. Eng. Sci. 38, 1993–2011.

Liew, K.M., Yang, J., Kitipronchai, S., 2003. Postbuckling of piezoelectric FGM plates subjected to thermo-electro-mechanical loading. Int. J. Solids Struct. 40, 3869–3892.

Nan, C.W., 1994. Magnetoelectric effect in composites of piezoelectric and piezomagnetic phases. Phys. Rev. B 50, 6082–6088.

Pan, E., 2001. Exact solution for simply supported and multilayered magneto-electro-elastic plates. J. Appl. Mech., ASME 68, 608–618.

Pan, E., Han, F., in press. Green's function for transversely isotropic piezoelectric functionally graded multilayered half spaces. Int. J. Solids Struct., doi:10.1016/j.ijsolstr.2004.11.003.

Pan, E., Han, F., 2005. Exact solution for functionally graded and layered magneto-electro-elastic plates. Int. J. Eng. Sci. 43, 321–339.

Pan, E., Heyliger, P.R., 2002. Free vibrations of simply supported and multilayered magneto-electro-elastic plates. J. Sound Vib. 252, 429–442.

Wang, X., Zhong, Z., 2003. A finitely long circular cylindrical shell of piezoelectric/piezomagnetic composite under pressuring and temperature change. Int. J. Eng. Sci. 41, 2429–2445.

Wang, J., Chen, L., Fang, S., 2003. State vector approach to analysis of multilayered magneto-electro-elastic plates. Int. J. Solids Struct. 40, 1669–1680.